Journal of Materials Chemistry A

ROYAL SOCIETY OF CHEMISTRY

PAPER

View Article Online
View Journal | View Issue

Cite this: J. Mater. Chem. A, 2025, 13, 275

Performance enhancement of aqueous ionic liquids with lower critical solution temperature (LCST) behavior through ternary mixtures†

Ahmed Mahfouz,[a] Andrew Z. Haddad,[b] Jordan D. Kocher[a] and Akanksha K. Menon*[a]

Thermally responsive ionic liquids (ILs) exhibit liquid–liquid phase separation when mixed with water and heated above a lower critical solution temperature (LCST), resulting in a water-rich (WR) and an IL-rich (ILR) phase. These binary IL–water mixtures can be employed in a variety of thermodynamic processes such as forward osmosis (FO) desalination, for which two solution properties are desirable: low phase separation temperature and high osmotic strength (osmolality). However, these two properties are interlinked, with ILs that exhibit higher osmotic strengths typically requiring higher phase separation temperatures. This behavior tends to arise from the hydrophilicity of the IL cations, which enhances osmotic strength while also elevating the phase separation temperature. In this work, we highlight a pathway to overcome this tradeoff by developing ternary IL mixtures (two ILs with varying cation hydrophilicity mixed with water), which lowers the phase separation temperature while maintaining and even enhancing the osmotic strength of the solution. We characterize the mixing behavior (osmolality, phase separation temperature, WR phase purity, and WR to ILR phase mass ratio) of four ILs as a function of their concentration in solution. We find that an enhancement of up to 81.6% in the osmolality with a concomitant reduction of up to 15.4% in the phase separation temperature can be achieved using this approach. The ternary mixture is also shown to improve the phase separation kinetics by nearly 95% compared to the binary mixture. Overall, this work highlights a new pathway to improve the performance of LCST ILs for water and energy applications.

Received 24th October 2024
Accepted 20th November 2024

DOI: 10.1039/d4ta07575g

rsc.li/materials-a

[a]George W. Woodruff School of Mechanical Engineering, Georgia Institute of Technology, Atlanta, GA 30332, USA. E-mail: akanksha.menon@me.gatech.edu

[b]Energy Storage and Distributed Resources Division, Lawrence Berkeley National Laboratory, Berkeley, CA 94720, USA

† Electronic supplementary information (ESI) available. See DOI: https://doi.org/10.1039/d4ta07575g

Akanksha K. Menon

Dr Akanksha Menon is an Assistant Professor in the Woodruff School of Mechanical Engineering at the Georgia Institute of Technology. She directs the Water – Energy Research Lab (https://amenonlab.me.gatech.edu/) that uses thermal science and functional materials to develop sustainable technologies for clean energy and water. Prior to this, she was a Rosenfeld Postdoctoral Fellow at Lawrence Berkeley National Laboratory and received a Ph.D. from Georgia Tech. Dr Menon is a recipient of the 2023 NSF CAREER Award, and the 2023 ACS Doctoral Young Investigator Award. Dr Menon was awarded the ASME Pi Tau Sigma Gold Medal in 2023, and she was featured by the U.S. Department of Energy in their Women @ Energy initiative.

Introduction

Separation processes are the essence of modern extractive technologies, with a wide range of applications including crude oil[1] and protein extraction,[1,2] uranium[1,3,4] and lithium recovery from aqueous mixtures,[1,3,5] mining and metallurgy,[6] carbon capture,[3,7,8] and desalination.[1,3,7,9] Ionic Liquids (ILs) are salts typically characterized by a melting point below 100 °C and are comprised of organic and/or inorganic cations and anions in over thousands of unique compositions.[10,11] ILs have garnered significant attention over the past decade for the aforementioned applications given their negligible vapor pressure, chemical and thermal stability, and high ionic conductivity.[8,12–15] These properties are a consequence of the inherent chemical structure differences between ILs and typical molecular liquids such as water or organic solvents – the steric hindrance arising from electrostatic forces between IL ions is significantly larger than van der Waals forces and hydrogen bonding in a molecular liquid, which results in low volatility, as well as chemical and thermal stability.[16] Owing to such unique properties, ILs have been used in the extraction of organic solvents[17,18] and metals,[19,20] as well as for carbon capture,[8] and freshwater production.[21–23]

A subset of ILs is thermally responsive in that they exhibit a liquid–liquid phase separation with water above a critical temperature. Ohno and co-workers first developed ILs that exhibit this phase behavior, referred to as the lower or upper critical solution temperature (LCST/UCST).[16,24–32] Fig. 1(a) illustrates the binodal phase diagram of ILs that exhibit LCST behavior. At a temperature $T_1 < T_C$ (where T_C is the critical temperature), the IL and water are fully miscible and form a single-phase homogenous solution at all concentrations w_{IL} (weight percent of IL in solution). At a temperature $T_2 > T_C$, the solution separates into a water-rich (WR) and IL-rich phase. Further heating the solution above T_2 increases the relative WR to ILR phase mass ratio (PMR), yielding higher purity WR and ILR phases. This increase in PMR and WR phase purity at higher temperatures is directly related to the width of the LCST phase diagram.

LCST ionic liquids are typically comprised of a cation and anion with hydrophilic and hydrophobic functional groups that lead to a temperature-induced phase separation when mixed with water. Fig. 1(c) illustrates this phase separation at a molecular level. At temperatures below T_C, the IL forms micelles with the hydrophilic heads bound to the water molecules that forms an ordered structure with strong intramolecular interactions (*i.e.*, hydrogen bonding). This ordering in aqueous solutions results in a negative entropy of mixing, and the enthalpy of mixing tends to be negative due to the strong cohesive interaction of the IL ions with each other and with water, resulting in exothermic heat release upon mixing.[33] Once the solution is heated above T_C, the entropy increases as the micelles break up exposing the hydrophobic tails that repel water, leading to microscopic aggregates that coalesce to form macroscopic WR and ILR phases.[34] Thermodynamically, the Gibbs free energy of mixing ($\Delta G_{mix} = \Delta H_{mix} - T\Delta S_{mix}$) of the IL–

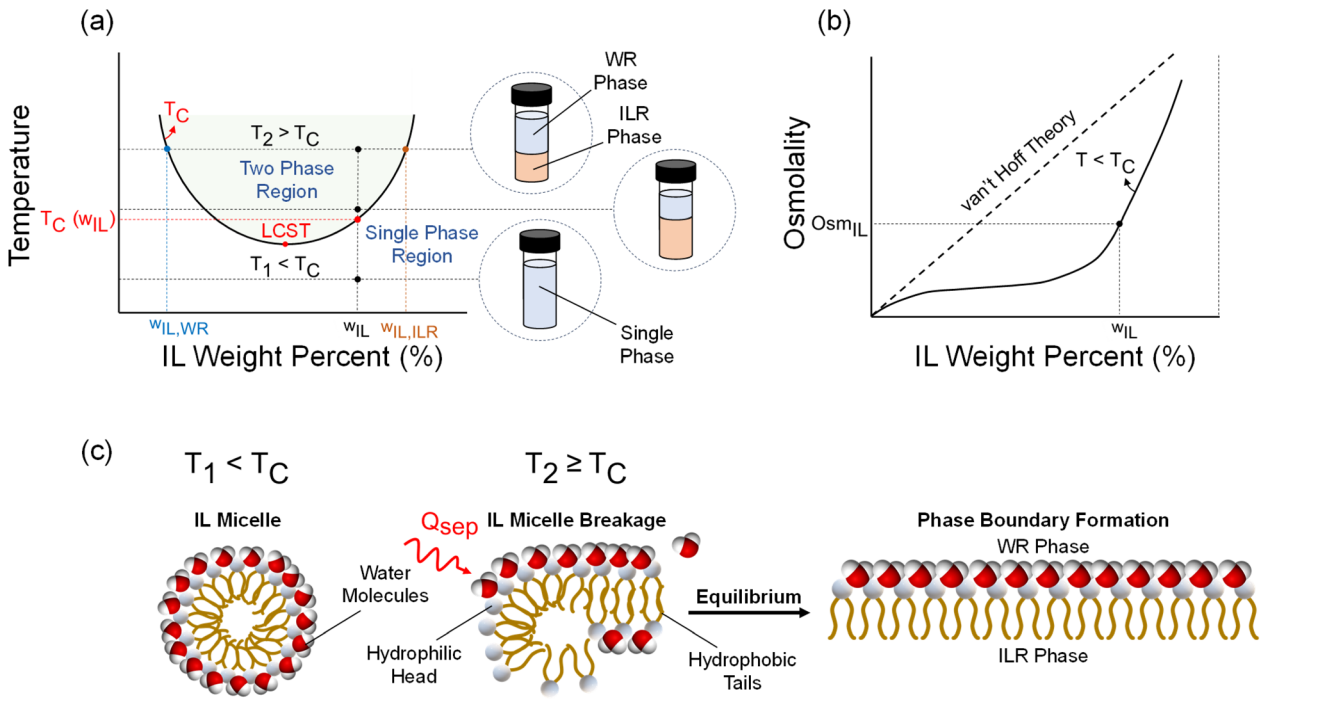

Fig. 1 Overview of LCST behavior. (a) Binodal phase diagram showing LCST behavior in IL–water mixtures. (b) Osmolality as a function of IL concentration in an aqueous solution at a temperature below T_C (single-phase mixture). (c) Illustration of IL–water micelle formation at temperatures below T_C, which upon heating causes the micelles to break and expose the hydrophobic tails of the IL, resulting in the formation of a phase boundary and two phases (WR and ILR).

water solution becomes positive (*i.e.*, IL mixing with water is unfavorable) above T_C at a given w_{IL} as a consequence of the $T\Delta S_{mix}$ term becoming more dominant than ΔH_{mix}. This transition of the free energy from negative to positive with a change in temperature is the thermodynamic driving force underlying this type of phase separation. The mechanism is also analogous to surfactants as evidenced by a lower surface tension of the IL solution relative to pure water at any given w_{IL}.[26,35] Above a critical concentration, the surface tension approaches a constant value and indicates the formation of micelle aggregates; this critical micelle concentration (CMC) phenomenon is only exhibited by ILs that are thermally responsive.[23,26]

Phase separation typically occurs below 60 °C for the majority of LCST-based ILs, and the corresponding separation enthalpy is ~5 J g^{-1}.[23,27] Owing to this low separation enthalpy (orders of magnitude lower than liquid–vapor phase change of water) and temperature, as well as the ionic nature of aqueous IL solutions, thermally responsive ILs have been used for applications such as forward osmosis (FO) desalination,[21–23,26,36] air conditioning, and dehumidification.[37–39] For FO desalination in particular, a hybrid membrane-thermal process for water treatment, LCST-based ILs are used as a draw solution.[21–23,26,36] Water spontaneously diffuses into the draw solution from a saline feed through a semi-permeable membrane until osmotic equilibrium is attained. The diluted draw solution is then heated above its critical temperature to induce liquid–liquid phase separation, after which the WR phase can be post-treated (nanofiltration) to yield high-purity water and minimize IL loss.[23] The efficacy of the draw solution for water extraction increases with osmotic strength – this is measured in terms of osmolality, with osmolality increasing monotonically with w_{IL} as illustrated in Fig. 1(b). However, these IL–water mixtures do not behave like dilute mixtures in that they do not follow van't Hoff solution theory due to the formation of IL aggregates through ion pairing (*i.e.*, a lower apparent number of free ions relative to an ideal solution).

The two key properties that dictate the performance of LCST-based ILs as draw solutions for FO desalination are: (i) a low regeneration temperature that depends on the phase diagram, and (ii) a high osmotic strength that depends on the number of "free" ions in solution. These properties enable the desalination of higher salinity feed solutions and/or increase the amount of water that can be recovered, while requiring low-grade heat to regenerate the two phases. The challenge, however, is that these parameters are coupled, with a higher osmotic strength often corresponding to a higher critical temperature for phase separation. This is a consequence of the fact that ILs with LCST behavior have a delicate balance of hydrophilic and hydrophobic ions – it comprises a cation that is nearly as hydrophilic as the anion is hydrophobic such that if either of the two moieties dominates, the IL will either be immiscible or fully miscible in water at all temperatures.[24] An LCST IL with greater overall hydrophilicity tends to have a higher osmotic strength and a higher phase separation temperature.[32] Saita *et al.* investigated the role of varying cation hydrophilicity and anion hydrophobicity on the phase separation temperature of $[P_{4444}]^+$ $[CF_3COO]^-$ and showed a strong proportional dependence of the phase separation temperature on the total hydrophilicity of the mixture.[31] Similar trends have also been reported for LCST hydrogels[40] and polymers.[41]

Tuning the performance of an LCST IL to attain a lower phase separation temperature without adversely impacting the osmotic strength may appear contradictory. In this work, we demonstrate a pathway to overcome this inherent limitation by developing ternary mixtures of two different ILs with water, where one IL has a more hydrophilic cation than the other. This results in a reduced critical temperature for phase separation while maintaining and/or even enhancing the osmotic strength of the solution as illustrated in Fig. 2. We characterize the mixing behavior of four different ILs with varying cation hydrophilicity (structure) and report its impact on the osmolality, phase separation temperature, relative WR to ILR phase mass ratio (PMR), and WR phase purity (properties) compared to the constituent binary ILs. We also investigate the kinetics of phase separation of these ternary mixtures, which has not been reported for any LCST ILs.

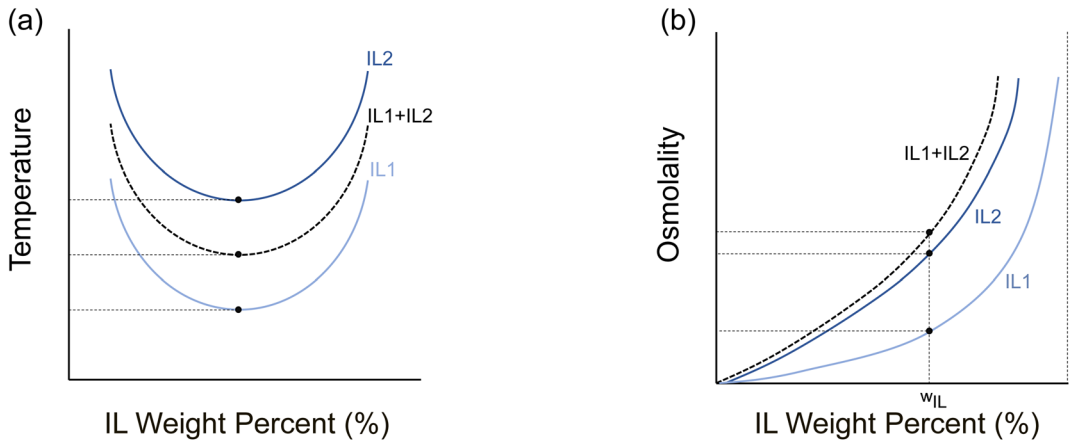

Fig. 2 Illustration of the effect of mixing two ILs with dissimilar phase diagrams and osmolality trends. (a) The IL mixture has a phase diagram that lies in between the two constituent ILs. (b) The osmotic strength of the IL mixture is higher than either of the constituent ILs.

Experimental

Materials

Four ILs were selected to investigate their mixing behavior as a function of the different cations and anions and develop structure–property relationships as shown in Fig. 3. The cations include tetrabutylammonium ($[N_{4444}]^+$) and tetrabutylphosphonium ($[P_{4444}]^+$); the anions include salicylate ($[Salicyl]^-$), 2,4-dimethylbenzene-sulfonate ($[DMBS]^-$), and trifluoroacetate ($[CF_3COO]^-$). We designate the ILs as follows: $[N_{4444}]^+$ $[Salicyl]^-$ is "NSal", $[P_{4444}]^+$ $[CF_3COO]^-$ is "PTFA", $[P_{4444}]^+$ $[Salicyl]^-$ is "PSal", and $[P_{4444}]^+$ $[DMBS]^-$ is "PDMBS". These ILs are solid at room temperature with a melting point around 60–80 °C. These ILs can be categorized into two groups – the phosphonium cation with three different hydrophobic anions, and the salicylate anion with two different hydrophilic cations.

Synthesis of ionic liquids

The PTFA and PDMBS ionic liquids were synthesized following the methodology reported in our previous work.[23] The NSal and PSal ILs were synthesized using a neutralization reaction.[23,26] Specifically, tetrabutylphosphonium hydroxide (TBPH) or tetrabutylammonium hydroxide (TBAH) (TCI America) and salicylic acid (TCI America) were used in an equal 1 : 1 molar ratio with a slight excess of the acid. Salicylic acid, owing to its low solubility in water at room temperature[42] was first diluted in excess DI water, heated at 80 °C, and stirred for three days until the salicylic acid was fully dissolved. To this, an equal molar amount of either TBAH or TBPH was added, turning the solution to a cloudy turbid color. The resulting solution was left to stir for two days at 70 °C, or until the solution pH was near 7 and the solution became clear. Upon completion of the reaction, the solution was cooled to room temperature and transferred to a separatory funnel, then extracted with dichloromethane (DCM) (Sigma Aldrich); this step was repeated three times. The organic DCM phase was collected and washed with water then extracted three times and then transferred to a rotary evaporator to remove DCM. The resulting ionic liquids were transferred to a oven and dried under vacuum at 90 °C for 48 hours to remove residual water. Upon removal of the ILs from the vacuum oven and cooling to room temperature, both ILs rapidly form a solid.

To confirm the synthesis of the NSal and PSal ionic liquids, the material was transferred to NMR tubes and dissolved in an NMR solvent for analysis. ^{1}H-NMR was performed (DMSO, δ/ppm relative to TMS): NSal: δ = 0.87–0.98 (12H; a), 1.23–1.36 (8H; b), 1.48–1.63 (8H, c), 3.10–3.21 (8H, d), 7.04–7.16 (1H, e), 6.52–6.62 (2H, f), 7.56–7.69 (1H, g); PSal: ^{1}H-NMR was performed that confirms the purity of the synthesized IL: (DMSO, δ/ppm relative to TMS): δ = 0.88–0.96 (12H; a), 1.25–1.35 (8H; b), 1.50–1.60 (8H, c), 3.11–3.20 (8H, d), 7.08–7.15 (1H, e), 6.55–6.65

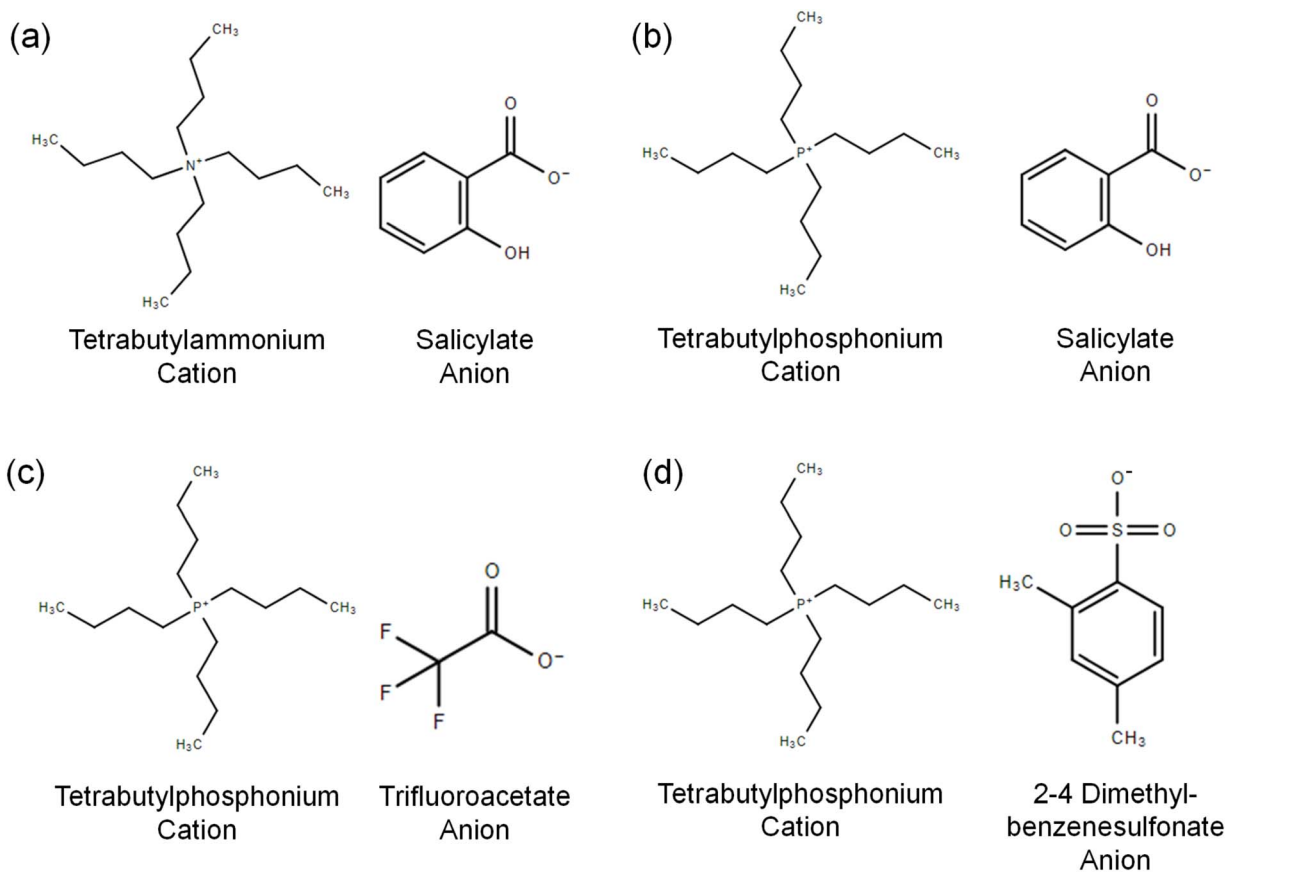

Fig. 3 Chemical structures of the ionic liquids studied in this work and their molar masses (M). (a) NSal (M_{NSal} = 364.11 g mol^{-1}). (b) PSal (M_{PSal} = 396.54 g mol^{-1}). (c) PTFA (M_{PTFA} = 372.02 g mol^{-1}). (d) PDMBS (M_{PDMBS} = 458.25 g mol^{-1}).

(2H, f), 7.59–7.70 (1H, g). The spectra are shown in Fig. S4(a) and (b),† and integration leads to results that are consistent with the target products for both ionic liquids. We note that the –OH proton present on the salicylate anion is notably absent in both spectra, which is consistent with prior reports on similar salicylate ILs.[42] To confirm the presence of the hydroxyl group, ATR-FTIR was performed, showing a strong hydroxyl stretching mode near 3300 cm^{-1} in Fig. S5† for both ionic liquids.

Characterization techniques

For all mixture characterization methods, a 10 g sample of IL in deionized water was prepared to obtain a range of IL concentrations with a maximum error of 0.01 g (0.1 wt% error in concentration).

Phase diagram. For each IL, the binodal curve was constructed by measuring the critical phase separation temperature at a given concentration using an optical cloud point measurement technique at a wavelength of 600 nm.[43] The measurement procedure is illustrated in Fig. 4(a), where the critical temperature corresponds to a drop in transmittance of <1%. Agilent Technologies Cary 5000 UV-Vis was utilized for all cloud point experiments with a temperature step of 0.5 °C every two minutes. The maximum error in the phase separation temperature is ±0.5 °C across all IL samples reported in this work.

Osmolality. The osmotic strength of the IL solutions at different concentrations can be assessed by measuring its osmolality, which is inversely proportional to the water activity (a_w) of the solution: Osm $kg^{-1} = -\ln(a_w)/V_w$, where V_w is the molar volume of pure water. For an IL solution at temperature $T < T_C$ at a given $w_{IL} > 0$, $a_w < 1$, due to vapor pressure of water in the solution being lower than the saturation pressure of pure water at that temperature (P_{sat}). To measure a_w, a chilled mirror dew point temperature technique was utilized. The initial vapor pressure of water in the chamber ($P^i_{W,chamber}$) is less than that of the solution ($P^i_{W,solution}$), and it increases until it is in equilibrium with the solution ($P^f_{W,chamber}$) as illustrated in Fig. 4(b). The AQUALAB 4TE water activity meter was utilized to measure the osmotic strengths of all the solutions in this work, with an a_w accuracy of ±0.003. For each sample, five measurements were taken and averaged, with a maximum standard deviation of 16% in osmolality.

Phase purity and separation kinetics. To characterize the purity of the WR phase of IL–water mixtures (binary and ternary), the solutions were heated to a separation temperature, $T_{sep} = 70$ °C for 30 minutes to induce phase separation. Given that the ILR phase is denser, it settles at the bottom while the WR phase floats on top – the PMR of WR to ILR was calculated by isolating and weighing each phase. The water activities were also measured to assess the purity of each phase.

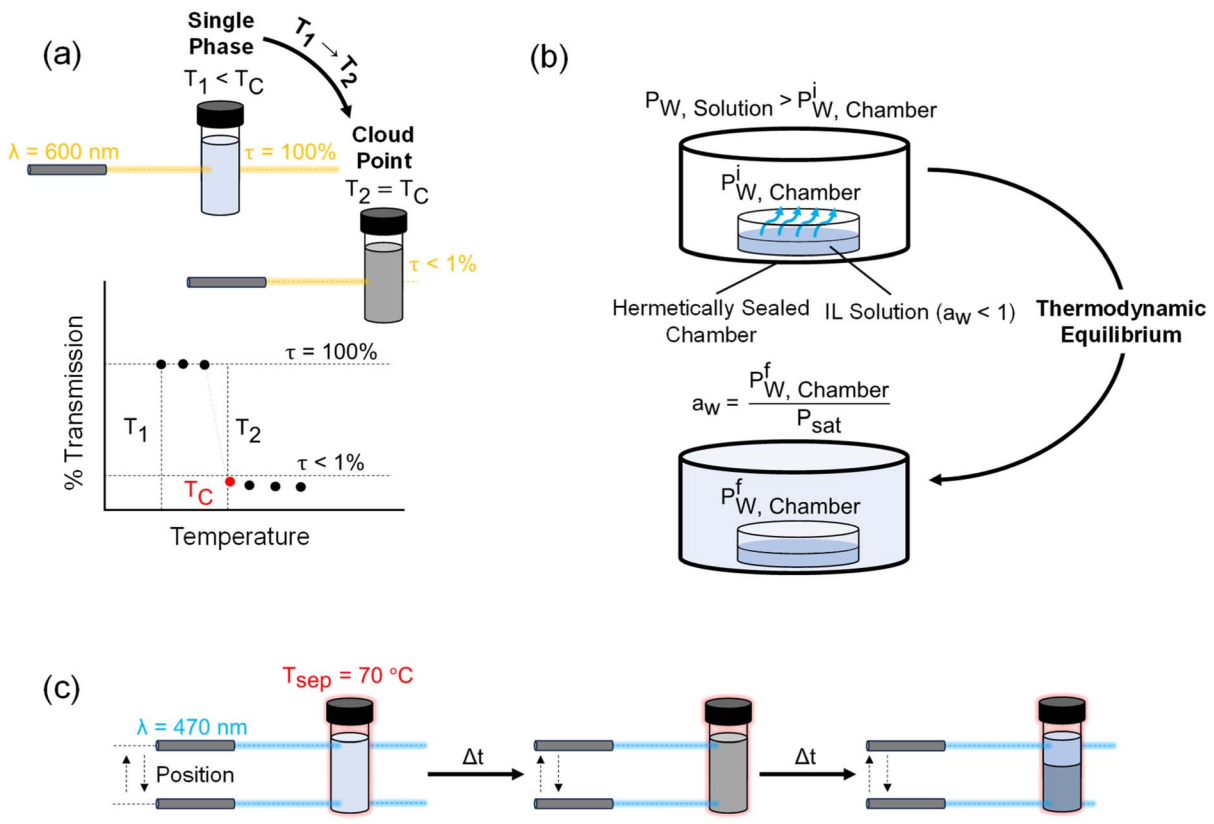

Fig. 4 Illustration of the characterization techniques utilized to measure thermodynamic properties of IL–water mixtures. (a) UV-Vis spectroscopy is used to perform transmittance measurements at a wavelength of 600 nm to construct the binodal phase diagram. (b) The osmotic strength of an IL solution and the purity of each phase are measured in terms of its water activity a_w, at 25 °C. (c) Position-variable transmission measurements at a wavelength of 470 nm to characterize phase separation kinetics.

To investigate the kinetics associated with the phase separation, experiments were performed by heating the IL (10 mL) to $T_{sep} = 70$ °C for 10–160 minutes by submerging each vial in an isothermal water bath, both with and without stirring at 500 rpm. Heating was also performed using a hotplate to provide a comparison to the water bath. To characterize the time required for complete phase separation, the DataPhysics MultiScan MS20 instrument was used to measure the position-variable light transmittance (along the height of the glass vial) at a wavelength of 470 nm while maintaining the sample at $T_{sep} = 70$ °C as illustrated in Fig. 4(c). This measurement (averaged over all positions for the WR phase) approaches a constant transmittance value which indicates that macroscopic phase separation is complete. The position-variable light transmittance measurements were performed at a spatial resolution of 0.055 mm and a temporal resolution of 10 seconds, and the maximum repeatability error of the 470 nm light source is ±0.05% of the measured transmittance at a given point.

Results and discussion

For forward osmosis desalination using LCST ILs, the relevant solution properties that dictate performance are the phase diagram, osmolality, WR phase purity, and the relative phase mass ratio (PMR). We first report these thermodynamic properties for binary mixtures (IL–water) for each of the four selected materials, namely NSal, PTFA, PDMBS, and PSal. Then, we present results for ternary mixtures (IL_1–IL_2–water), which includes NSal + PTFA, PTFA + PDMBS, and NSal + PSal with the goal of establishing structure–property relationships and design rules. Finally, we discuss the kinetics associated with the phase separation for both binary and ternary LCST mixtures given its importance for a realistic desalination application.

Binary mixtures of IL–water

Fig. 5(a) shows the experimentally measured phase diagrams for NSal, PTFA, PDMBS, and PSal. To enable facile phase separation and regeneration in the FO desalination process, a lower LCST corresponding to a low-grade heat source is desirable. Owing to the greater hydrophilicity of the ammonium cation, NSal has the highest LCST and critical phase separation temperature at all concentrations compared to the three phosphonium-based ILs.[31] For a given cation, the phase diagrams are ordered inversely with respect to the hydrophobicity of the anion – the more hydrophobic the anion, the lower the phase separation temperature.[26] Accordingly for ILs with the phosphonium cation, since the anion hydrophobicity decreases as $[Salicyl]^-$, $[TFA]^-$, $[DMBS]^-$, the LCSTs increase as PSal, PTFA, and PDMBS. The phase diagrams reported in Fig. 5(a) are in agreement with previous reports by Kamio *et al.* and Haddad *et al.*[23,26]

The osmolality of the four ILs is shown in Fig. 5(b). To enable FO desalination of saline feeds and/or to increase the water flux (an water recovery), a higher osmolality is desirable. Below 50 wt% IL concentration, NSal, PSal, and PDMBS have comparable osmolalities. On the other hand PTFA, despite having a less hydrophilic cation than NSal and a more hydrophobic anion than PDMBS, has a higher osmolality than the other ILs at concentrations below 50 wt%. This suggests that the osmotic strength of IL–water mixtures cannot just be tied to the hydrophobic–hydrophilic balance in the chemical structure, and it is also impacted by ion clustering within the solution as illustrated in Fig. 1(c).[34] Specifically, the relatively low and near-constant osmolality trend at lower IL concentrations has been attributed to the formation of "microemulsion-like" aggregates that reduce the number of free ions in the solution and hence decrease the apparent osmolality of the IL solution.[26,44–46] These micelle aggregates however are necessary for temperature-induced phase separation as illustrated in Fig. 1(c); as such, the osmolality trend between 20–50 wt% shown in Fig. 5(b) corresponds to the relatively flat region of the phase diagrams in Fig. 5(a). Above 50 wt%, the phase diagram increases monotonically and so does the IL osmolality. This suggests an increase in the number of free ions in the IL solution at higher concentrations, which comes at the cost of a higher phase separation temperature. The osmolality trends reported herein are consistent with previous reports by Kamio *et al.* and Haddad *et al.*[23,26]

Another important property is the WR phase purity after thermal separation. From an application standpoint, a higher WR phase purity is desirable as it minimizes the need for post-treatment steps. This depends primarily on the width of the phase diagram and is determined by the concentration of residual IL in the WR phase, $w_{IL,WR}$, at temperatures above T_C. For the four ILs, the width of the phase diagram decreases from PDMBS to PSal, NSal, and PTFA. As such, the purity of the WR phase follows the same order as shown in Fig. 5(c) from the most pure (lowest osmolality) being PDMBS to the least pure (highest osmolality) being PTFA and NSal. The WR phase purity is characterized by heating at $T_{sep} = 70$ °C for 30 minutes in a water bath that provides uniform (volumetric) heating for phase separation. We note that from a thermodynamic perspective (at equilibrium), the purity of the WR phase should be independent of the initial IL concentration in the mixture and should only vary with the residual IL concentration in the WR phase. However, kinetic and temporal effects have a non-negligible effect on the experimentally measured purity of the WR phase (see ESI Note 4†).

Apart from purity, the amount of the WR phase that can be regenerated varies both as a function of IL concentration and the specific IL species as a consequence of the phase diagram lever rule. From an application standpoint, a higher PMR is desirable as it maximizes the amount of water produced. The phase mass ratio of the four IL–water mixtures is shown in Fig. 5(d), with all mixtures exhibiting a monotonic decrease with concentration. This trend follows the phase diagram trend: the more hydrophobic the anion, the lower the PMR. As such, NSal has the lowest PMR at a given concentration, followed by PSal, PTFA, and PDMBS, owing to the anions' decreasing hydrophobicity as $[Salicyl]^-$, $[TFA]^-$, and $[DMBS]^-$. Although the ammonium-based cation in NSal is more hydrophilic than the phosphonium-based cation in the PSal, both ILs exhibit a nearly identical PMR trend. This suggests that the PMR is a strong

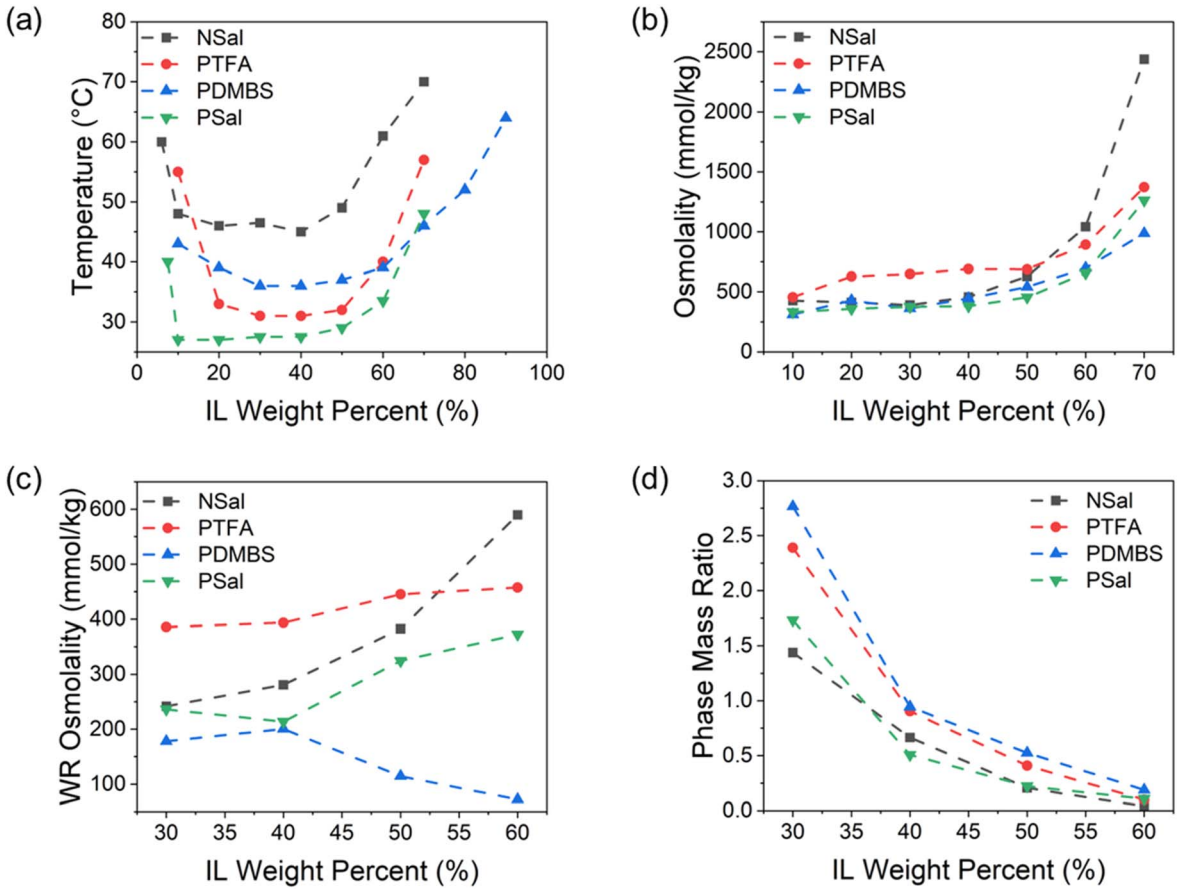

Fig. 5 Properties of NSal, PTFA, PDMBS, and PSal binary mixtures with water showing (a) phase diagram, (b) osmolality, (c) WR phase osmolality (phase purity), and (d) WR to ILR phase mass ratio (PMR). The data in (c) and (d) is based on phase separation at $T_{sep} = 70$ °C for 30 minutes in a water bath. All osmolality measurements shown in (b) and (c) are based on five water activity measurements with a maximum standard deviation of ±16% in osmolality. The maximum error in the cloud point measurements for T_C shown in (a) is 0.5 °C. The maximum error in the PMR measurements shown in (d) is 0.1%.

function of the anion hydrophobicity and only weakly correlated with the cation hydrophilicity. This can be connected to the molecular phase separation mechanism illustrated in Fig. 1(c), where the hydrophobic anion tail is directly responsible for the phase boundary formation. Accordingly, the higher PMR with a less hydrophobic anion can be attributed to the lower electrostatic repulsion force that a water molecule experiences as it migrates into the WR phase.[47,48] It is also worth noting that phase separation at concentrations ≥70 wt% does not yield a continuous WR phase, and instead results in dispersed WR droplets in the ILR phase. This explains why the PMR for binary IL–water solutions above 60 wt% tends towards zero in Fig. 5(d).

Overall, as the results in Fig. 5(a) and (b) illustrate, the osmotic strength and critical phase separation temperature of binary mixtures are tied to the overall hydrophilicity of the solution, with higher osmotic strengths coming at the cost of higher phase separation temperatures. On the other hand, the purity of the WR phase and the PMR of a binary mixture depend on the width of the phase diagram and the hydrophobicity of the anion, respectively, as illustrated in Fig. 5(c) and (d). This establishes structure–property relationships for binary mixtures of thermally responsive ILs that are relevant for desalination applications.

Ternary mixtures of IL_1–IL_2–water

Ternary mixtures are a pathway to overcome the interlinked properties of thermally responsive ILs such as NSal, PTFA, PDMBS, and PSal when mixed with water. The underlying hypothesis is that a mixture of two ILs (IL_1 and IL_2) with different cation hydrophilicity can exhibit a synergistic effect – simultaneous increase in osmolality and decrease in the phase separation temperature over certain concentrations while maintaining or improving the purity of the WR phase and the PMR. In this section, we report this behavior and map out the ternary mixture compositions where this effect can be leveraged. Table 1 shows the different ternary mixture compositions that were investigated in this work, with the last column representing the fraction of IL_1 (first column) relative to the total IL (third column) within the solution: $\frac{w_{IL_1}(\%)}{w_{IL_1}(\%) + w_{IL_2}(\%)}$.

Three different IL mixtures were investigated, namely NSal + PTFA, PTFA + PDMBS, and NSal + PSal. In this section we present the experimental results for NSal + PTFA as this shows

Table 1 Ternary mixture compositions for ILs characterized in this work

IL_1 weight percent (%)	IL_2 weight percent (%)	Total IL weight percent (%)	IL_1 weight fraction
20	10	30	0.67
10	20	30	0.33
25	15	40	0.63
15	25	40	0.38
25	25	50	0.50
30	25	55	0.55
25	30	55	0.45
30	30	60	0.50

the most promising performance, while data for PTFA + PDMBS and NSal + PSal are in ESI Notes 2 and 3,† respectively. Fig. 6 shows the thermodynamic properties of the NSal + PTFA ternary mixtures as a function of the total IL weight% in solution (x-axis) and the weight fraction of NSal within this (y-axis). This allows for a direct comparison of a ternary mixture's performance relative to its two constituent ILs, NSal, and PTFA ($y = 0$ and $y = 1$ represent binary mixtures of PTFA and NSal with water, respectively).

The osmolality of the NSal + PTFA ternary mixture is illustrated in Fig. 6(a). At a composition of 40 wt% total IL (15 wt% NSal + 25 wt% PTFA), the osmolality is 831.8 ± 27.8 mmol kg^{-1}, which is 81.4% higher than that of a 40 wt% NSal binary mixture and 20.6% higher than a 40 wt% PTFA binary mixture. Furthermore, the phase separation temperature at this ternary composition is 39 °C, which is 6 °C lower than 40 wt% NSal, but 8 °C higher than 40 wt% PTFA as shown in Fig. 6(b). The ternary mixture of NSal with PTFA thus follows the qualitative trend illustrated in Fig. 2, where the osmolality is higher than both constituent ILs while the phase separation temperature lies in between the two ILs. This behavior is found to be generally true for mixtures of two thermally responsive ILs as shown for NSal + PSal as well (ESI Note 2†). However, in the particular case of PTFA + PDMBS mixtures, owing to their similar phase diagrams (LCSTs of 31 °C *vs.* 36 °C, respectively), and common phosphonium-based cation, the synergistic effect is much less

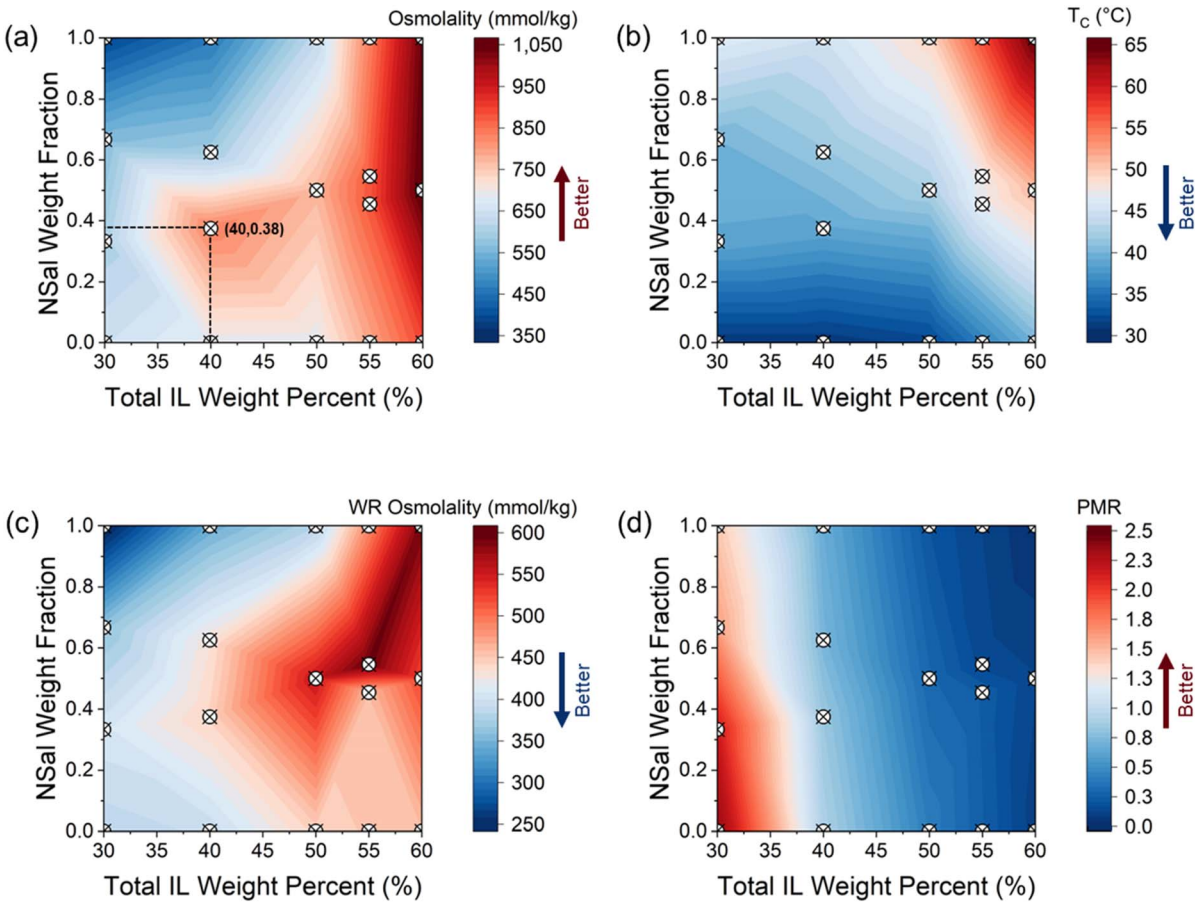

Fig. 6 Thermodynamic properties of the NSal + PTFA ternary mixtures in terms of the weight fraction of NSal with respect to the total IL in the solution (y-axis) and the total IL weight percent (x-axis) at the compositions shown in Table 1. (a) Osmolality, (b) critical phase separation temperature, (c) WR phase osmolality, and (d) WR to ILR phase mass ratio (PMR). All the data in (c) and (d) is based on a phase separation of T_{sep} = 70 °C for 30 minutes in a water bath. All osmolality measurements shown in (a) and (c) are based on five water activity measurements with a maximum standard deviation of ±16% in osmolality. The maximum error in the cloud point measurements for T_C shown in (b) is 0.5 °C. The maximum error in the PMR measurements shown in (d) is 0.1%. The marked points correspond to measured data points at the coordinates listed in Table 1.

pronounced. The phase separation temperatures of the PTFA + PDMBS mixtures are 4–6 °C lower than PDMBS at any given total IL concentration owing to the addition of PTFA with a lower LCST, but the osmolality of this ternary mixture remains relatively unchanged (ESI Note 3†).

The WR phase purity of the NSal + PTFA mixtures does not exhibit an improvement over its precursor ILs as illustrated in Fig. 6(c) given their similar phase diagram widths. Specifically, at 40 wt% total IL, the WR phase purity of this mixture is 444.0 ± 51 mmol kg^{-1}, which is 29.3% and 12.8% higher than a 40 wt% NSal or PTFA alone, respectively. However, in the case of PTFA + PDMBS and NSal + PSal, the WR phase is improved compared to the constituent IL with the narrower phase diagram. This is attributed to the wider phase diagrams of PDMBS and PSal relative to NSal and PTFA (see ESI Notes 2 and 3†). The PMR of the NSal + PTFA mixtures exhibits a small improvement as evidenced by the nearly parallel contours shown in Fig. 6(d). The contours are slightly skewed to the right as the NSal concentration is reduced and $y = 0$ is approached (*i.e.*, pure PTFA). The 15 wt% NSal + 25 wt% PTFA mixture exhibits a PMR of 0.83, corresponding to a 24% increase over a 40 wt% NSal solution.

To better understand the mixing behavior of NSal and PTFA, the two ILs are mixed at different ratios, $r = \frac{w_{\mathrm{NSal}}\ (\%)}{w_{\mathrm{PTFA}}\ (\%)}$ to yield total IL weight percents from 10–70 wt%. Four different mixing ratios are investigated: 0.6, 1.0, 1.67, and 2.0. Fig. 7 shows the phase diagrams and the osmolality trends of the mixtures relative to the two binary NSal-water and PTFA-water mixtures at the same total IL weight percentages. The ternary mixtures always exhibit a higher osmolality than either precursor IL across all weight concentrations below 70 wt%, as illustrated in Fig. 7(b). This higher osmolality is also accompanied with a phase separation temperature that falls in between the two precursor ILs, as shown in Fig. 7(a). As such, the mixing ratio of the two ILs does not impact the observed synergistic effect for these ternary mixtures.

These results validate the hypothesized behavior illustrated in Fig. 2, where mixing two ILs with different LCSTs results in a ternary mixture that possesses a higher osmotic strength than either IL while maintaining an intermediate phase separation temperature. This synergistic interaction arises when there is a difference in the LCST and osmolality between the ILs in the ternary mixture. Owing to the greater LCST difference between NSal and PTFA (14 °C) relative to PTFA and PDMBS (5 °C), the osmolality peaks at a composition of 15 wt% NSal + 25 wt% PTFA, whereas the osmolality of the 15 wt% PTFA + 25 wt% PDMBS mixture exhibits no improvement over its precursor ILs (see ESI Note 3, Fig. S2(a)†) at the same total IL concentration of 40 wt%. The purity of the WR phase and PMR on the other hand are directly proportional to the width of the phase diagram. As such, mixing two ILs with different phase diagram widths results in an improved WR phase purity. Accordingly, owing to the dissimilar widths of PTFA relative to PDMBS and NSal relative to PSal, the WR phases of the 15 wt% PTFA + 25 wt% PDMBS (see ESI Note 3, Fig. S2(c)†) and 25 wt% NSal + 15 wt% PSal (see ESI Note 2, Fig. S1(c)†) mixtures are purer than their precursor IL at the same total IL concentration of 40 wt%. These observations form the basis of design rules for ternary mixtures of thermally responsive ILs, as discussed later.

Mechanism for performance enhancement using ternary mixtures

To understand what leads to the superior performance of ternary mixtures, we first evaluate if they adhere to (i) ideal thermodynamic mixing laws, or to (ii) a weighted average model (on both a mass and molar basis) of the binary mixture ILs. If the mixtures adhered to an ideal entropy of mixing model (*i.e.*, positive entropy of mixing), the chemical potential of water (and therefore the water activity and osmolality) in a ternary mixture at a given total IL concentration would be equal to that of a binary mixture at that same total IL concertation (see ESI Note 6† for a detailed derivation). This however is contrary to the observed behavior of all ternary mixtures, particularly NSal + PTFA shown in Fig. 7(b), which has a higher osmolality than its constituent binary ILs. Additionally, ternary mixtures cannot be described as simple physical mixtures that obey a weighted

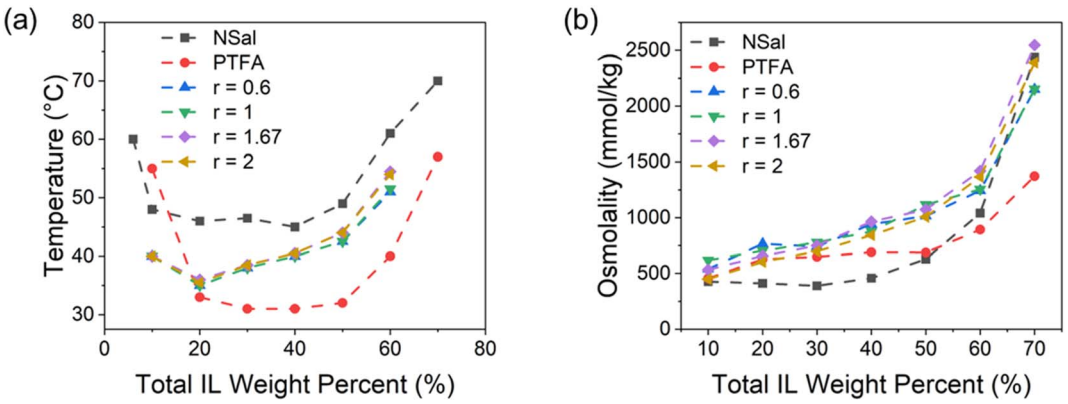

Fig. 7 Properties of NSal + PTFA ternary mixtures as a function of different weight ratios, *r*. (a) Phase diagrams of the mixtures as well as pure NSal and PTFA. (b) Osmolality of the ternary mixtures as well as pure NSal and PTFA. All osmolality measurements shown in (b) are based on five water activity measurements with a maximum standard deviation of ±16% in osmolality. The maximum error in the cloud point measurements for T_C shown in (a) is 0.5 °C.

average model of the two constituent ILs. This is because a weighted average of the properties of two binary mixtures (IL_1 + water) and (IL_2 + water) on a mass or molar basis fails to reproduce the phase diagrams and the osmolality trends for any of the three ternary systems (IL_1 + IL_2 + water) reported in this work (see ESI Note 7† for a detailed derivation). These observations suggest that there are strong non-ideal interactions at the molecular level between the two ILs within a ternary mixture, in addition to the non-ideal interaction of each IL with water.

One potential mechanism that explains the observed enhancement in osmolality and the concomitant reduction in T_C in these ternary mixtures is the formation of ion cluster networks, as illustrated in Fig. 8. It has been shown in the literature that when multiple ions are mixed in an aqueous solution, favorable interaction between some ion pairs may lead to the formation of branched cluster networks.[49] We hypothesize that this is the underlying structure–property relationship in ternary mixtures: when two ILs are mixed with water, one of the anionic and/or cationic pairs forms an ordered structure, which in turn lowers the entropy of mixing (more negative) and the resulting T_C. The favorability for the formation of such networks increases when ILs with dissimilar cation and anion pairs are combined, since the electrostatic repulsion is lower. This is why NSal + PTFA that has dissimilar cation/anion pairs exhibits a reduction in T_C, compared to PTFA + PDMBS or NSal + PSal that have common anions. This is also consistent with the fact that ion association is directly related to hydrophobicity[50] – given that the hydrophobicity of the anions decreases as: $[Sal]^-$, $[TFA]^-$, and $[DMBS]^-$, the NSal + PTFA ternary system exhibits the greatest synergy.

Ion clustering (non-ideal interaction) can also explain how lower T_C values and higher osmolalities can simultaneously exist in ternary mixtures. Specifically, if ion cluster networks did not form, an increase in osmolality would require an increase in the number of free ions, which would translate to an increase in the entropy of mixing (higher T_C) and *vice versa*. One way that this seemingly contradictory behavior can be resolved is if the number of free water molecules is lower in a ternary mixture due to water entrapment and solvation within the ion cluster networks. In effect, this lowers both the entropy of mixing and water activity, resulting in a lower T_C and higher osmolality.

This interaction between the two ILs and with water enables ternary mixtures to overcome the inherent phenomenological tradeoff that is typical of binary ILs, where a higher osmotic strength is tied to a higher T_C. Ternary mixtures thus provide a unique pathway for enhancing the physical properties of known LCST materials given that the discovery of new thermally responsive ionic liquids is extremely challenging. The hypothesized ion clustering framework provides a first step towards understanding the structure–property relationships in ternary LCST mixtures. Future studies using molecular dynamics (MD) simulations are necessary to validate this hypothesis by quantifying which ion pairs form cluster networks, as well as the size and number of such networks. However, this area of computational research requires significant development even for binary IL–water mixtures that are thermally responsive, with recent reports on the use of MD to investigate water diffusion into PDMBS[51] and to describe the non-ideal osmotic behavior of PTFA and PDMBS.[23,34,52]

Phase separation kinetics

Finally, the phase separation kinetics of ternary mixtures are investigated and compared to binary IL–water mixtures to provide insight into how stirring and heating mode impact the purity of the WR phase. This is important from an application

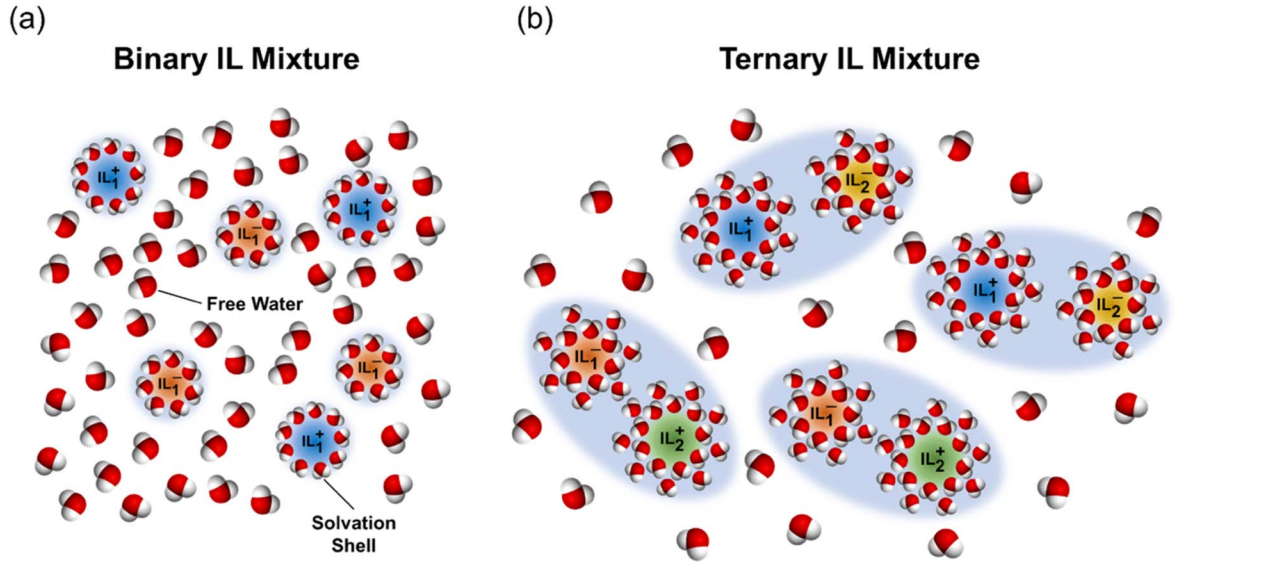

Fig. 8 Illustration of the hypothesized ion association interaction mechanism between two IL species in a ternary mixture that promotes a decrease in T_C coupled with an increase in osmolality. (a) Binary IL mixtures. (b) Ternary IL mixtures. The decrease in the number of free water molecules through solvation within the ion clusters results in an increase in osmolality, while further decreasing the entropy of mixing due to increased molecular ordering, effectively lowering T_C.

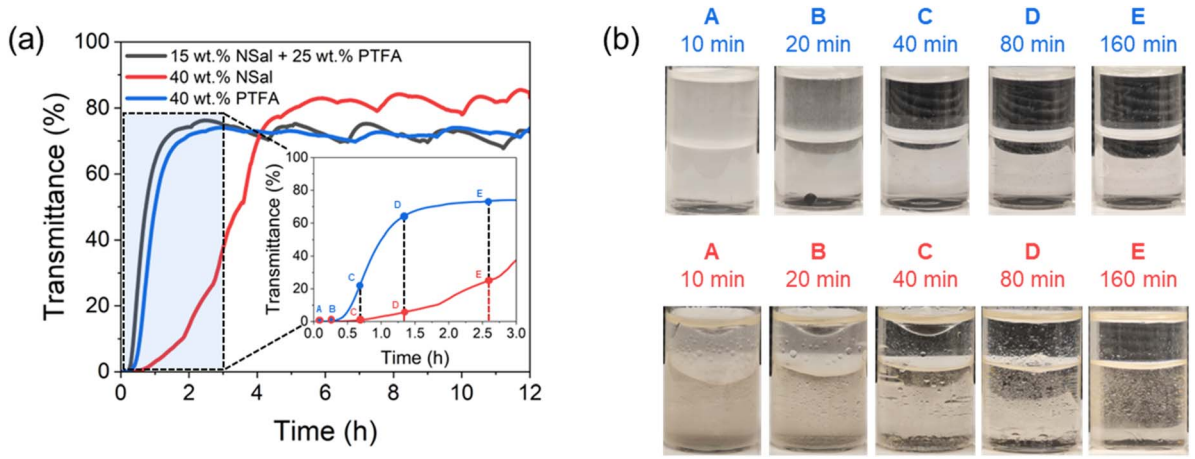

Fig. 9 Phase separation kinetics of 40 wt% NSal, 40 wt% PTFA, and 15 wt% NSal + 25 wt% PTFA at $T_{sep} = 70$ °C. (a) Position-variable transmission averaged over all positions along the WR phase at 470 nm; inset shows 40 wt% NSal and 40 wt% PTFA data during the first three hours. (b) Phase separation as a function of time for 40 wt% PTFA and 40 wt% NSal based on the points labeled on the inset shown in (a). Position-variable light transmittance measurements were performed at a spatial resolution of 0.055 mm and a temporal resolution of 10 seconds, and the maximum repeatability error of the light source is ±0.05% of the measured transmittance at a given point.

standpoint as it dictates the time required for the two macroscopic phases to form to yield the WR and ILR components that represent the clean water product and the recycled draw solution. A phase separation temperature of 70 °C was used for all ILs (NSal, PTFA, PDMBS, and PSal) at 40 wt% for binary mixtures as well as for the ternary IL mixtures at the optimal composition identified previously (15 wt% NSal + 25 wt% PTFA, 15 wt% PTFA + 25 wt% PDMBS, and 25 wt% NSal + 15 wt% PSal). The WR phase purity results are shown in ESI Note 4 (see Fig. S3†) and suggest that the purity of the WR phase is adversely impacted with stirring. This is a consequence of the scattering and intermixing of the WR and ILR layers with stirring, which disrupts the phase separation process by prolonging coalescence. As a result, the formation of two macroscopic phases is prevented until the stirring is switched off. Additionally, phase separation must be induced using uniform isothermal heating from all sides (*e.g.*, in a water bath instead of with a hot plate) for the duration needed to achieve full phase equilibration. The exact time varies depending on the particular IL species as illustrated in Fig. 9. Such findings enable the optimization of system-level designs employing LCST ILs as draw solvents.

To quantify the phase separation rate, light transmittance at 470 nm is averaged over the thickness (height) of the WR phase for 12 hours for 40 wt% PTFA (blue line), 40 wt% NSal (red line), and 15 wt% NSal + 25 wt% PTFA (dark grey line). As shown in Fig. 9(a), the spatially averaged transmittance of the WR phase for this ternary mixture and the PTFA binary mixture increased at a rate of 39% h^{-1} compared to 20% h^{-1} for the 40 wt% NSal binary mixture – this is approximately a 2× improvement in the time taken. The difference is illustrated in Fig. 9(b) for 40 wt% PTFA and NSal solutions at specified time intervals corresponding to the inset of Fig. 9(a). The difference in phase separation rates can be seen at the 160 minute mark (point E) in Fig. 9(b), where both phases of PTFA are transparent, whereas the bottom (ILR) phase of NSal is noticeably cloudy, indicating incomplete macroscopic phase separation. This is captured by the change in transmittance of the WR phase for 40 wt% NSal even after 160 minutes (point E) as shown in Fig. 9(a).

We note that the separation times reported in Fig. 9(a) are not only a function of the IL species but also depend on the geometry of the container used. The phase separation times reported herein correspond to a sample volume of 10 mL and a height of 5 cm. Iwasawa *et al.* experimentally demonstrated that the ILR phase forms a discontinuous phase within a continuous WR phase upon heating above T_C.[27] As such, Stokes law dictates the settling time of the ILR phase based on the vertical distance traveled to reach the phase boundary. For a given sample volume, the container geometry thus impacts the settling distance traversed by the ILR phase, in effect, varying the phase separation time.

Conclusion

For binary LCST IL–water mixtures, the solution properties are predominantly dependent on the hydrophilic and hydrophobic moieties of the IL, with greater osmotic strength being accompanied by higher phase separation temperatures. This fundamental barrier for binary mixtures can be overcome through ternary mixtures of two ILs with water, where one IL is of greater overall hydrophilicity than the other, in effect lowering the phase separation temperature while maintaining or enhancing the osmotic strength of the mixture over its constituents. A purer WR phase can be attained using ILs that exhibit wider phase diagrams, while a higher PMR at a given IL concentration and separation temperature can be regenerated using ILs with less hydrophobic anions. Mixing two ILs with dissimilar phase diagram widths in a ternary mixture will enhance the purity of the WR phase over the IL with the narrower phase diagram, while the ternary mixture's PMR will exhibit an intermediate trend relative to either IL. In summary, this work establishes the following empirical design rules for ternary IL mixtures that demonstrate enhanced performance compared to binary mixtures for FO desalination:

• To improve the phase separation behavior, *i.e.*, to lower the LCST for facile thermal separation, two ILs that have a large difference in their LCST values, should be mixed. For example, the 15 wt% NSal + 25 wt% PTFA (40 wt% total IL) ternary system achieves a T_C of 39 °C compared to a 40 wt% NSal (T_C of 45 °C) and 40 wt% PTFA (T_C of 31 °C) binary systems.

• To improve the osmotic strength, *i.e.*, to raise the osmolality for higher water flux ro recovery, two ILs that have a large difference in their water activity should be mixed. For example, the 15 wt% NSal + 25 wt% PTFA (40 wt% total IL) ternary system achieves an osmolality of 831.8 mmol kg^{-1}, which is ∼82% higher than the 40 wt% NSal and ∼21% higher than the 40 wt% PTFA binary systems.

• To improve the WR phase purity and PMR, *i.e.*, to obtain high-purity clean water, two ILs with dissimilar phase diagram widths should be mixed. For example, the 25 wt% NSal + 25 wt% PSal (50 wt% total IL) ternary system exhibits a higher WR phase purity (2× lower osmolality) than its constituent binary ILs and a higher PMR. A similar effect is also observed for the 25 wt% PTFA + 25 wt% PDMBS (50 wt% total IL) ternary system.

Phase separation kinetics can also be enhanced through ternary IL mixtures, nearly doubling the rate in the case of 15 wt% NSal + 25 wt% PTFA relative to 40 wt% NSal. These enhancements in performance can be leveraged for FO desalination applications—ternary IL mixtures as draw solutions can harness low-grade heat for phase separation owing to their lower critical temperatures, while simultaneously enhancing water flux (or desalinate a more saline source) owing to their higher osmotic strength. Specifically, the ∼2× osmolality enhancement of the ternary mixture (15 wt% NSal + 25 wt% PTFA) demonstrated herein compared to a binary mixture with the same total IL concentration (40 wt% NSal) translates to the desalination of a 24 g L^{-1} salinity feed compared to 13 g L^{-1}, while undergoing phase separation at a temperature that is 6 °C lower than the binary mixture. Overall, this work lays the foundation for a pathway to tune the performance of LCST ILs for various applications that require different temperature and osmotic strength constraints. Future efforts should focus on providing mechanistic insight into the underlying molecular interactions (such as the hypothesized ion cluster networks) that improve performance using computational approaches (*e.g.*, using MD), as well as experimental tools to characterize the structural dynamics (*e.g.*, using X-ray scattering). This will be important to understand these thermally responsive mixtures, given that weighted average or ideal entropy of mixing models fail to capture the behavior of ternary IL–water mixtures.

Data availability

The data supporting this article have been included as part of the ESI.†

Author contributions

Conceptualization: AKM. Methodology: AM, AZH, JDK, and AKM. Investigation: AM and AZH. Visualization: AM and JDK. Resources: AKM and AZH. Writing – original draft: AM and AKM. Writing – review & editing: AM, JDK, AZH, and AKM.

Conflicts of interest

J. D. K. is the inventor on an international patent (application number PCT/US2023/065629, patent pending), a U.S. patent (application number 18/298796, patent pending), and a provisional patent, which describe various uses of LCST materials in air conditioning cycles. A. K. M and A. Z. H are co-inventors on U.S patent number 11845682 that describes the use of binary and ternary LCST materials for desalination. The authors declare that they have no other competing interests.

Acknowledgements

Experiments were performed in part at the Georgia Tech Institute for Electronics and Nanotechnology, a member of the National Nanotechnology Coordinated Infrastructure (NNCI), which is supported by the National Science Foundation (Grant ECCS-2025462). J. D. K. acknowledges financial support from the IBUILD Fellowship. A. Z. H. acknowledges funding from LBNL LDRD grant and the U.S. Department of Energy's Solar Energy Technologies Office (SETO) under award No. 34324. Work at the Molecular Foundry (LBNL) was supported by the U.S. Department of Energy's Office of Basic Energy Sciences under contract No. DE-AC02-05CH11231. A. K. M acknowledges the Woodruff School of Mechanical Engineering at Georgia Tech for startup funds used to perform this work. The authors would also like to thank Hieu Ngo and Paul Simutis from DataPhysics for assistance with the MS20 system.

References

1 D. S. Sholl and R. P. Lively, Seven chemical separations to change the world, *Nature*, 2016, **532**(7600), 435–437.
2 J. A. Asenjo and B. A. Andrews, Aqueous two-phase systems for protein separation: phase separation and applications, *J. Chromatogr. A*, 2012, **1238**, 1–10.
3 D. S. Sholl and R. P. Lively, Exemplar mixtures for studying complex mixture effects in practical chemical separations, *JACS Au*, 2022, **2**(2), 322–327.
4 M. Srncik, *et al.*, Uranium extraction from aqueous solutions by ionic liquids, *Appl. Radiat. Isot.*, 2009, **67**(12), 2146–2149.
5 Y. Sun, *et al.*, Recent advances in magnesium/lithium separation and lithium extraction technologies from salt lake brine, *Sep. Purif. Technol.*, 2021, **256**, 117807.
6 S. R. Izatt, R. L. Bruening and N. E. Izatt, Metal separations and recovery in the mining industry, *JOM*, 2012, **64**, 1279–1284.
7 R. A. Bartsch and J. D. Way, *Chemical Separations with Liquid Membranes: An Overview*, ACS Symposium Series, 1996, ch. 1, vol. 642, pp. 1–10.
8 S. Zeng, *et al.*, Ionic-liquid-based CO2 capture systems: structure, interaction and process, *Chem. Rev.*, 2017, **117**(14), 9625–9673.

9 M. Al-Shammiri and M. Safar, Multi-effect distillation plants: state of the art, *Desalination*, 1999, **126**(1–3), 45–59.
10 Q. Zhao and J. Anderson, Ionic Liquids, *Comprehensive Sampling and Sample Preparation*, 2012, vol. 2, pp. 213–242.
11 C. Chiappe and D. Pieraccini, Ionic liquids: solvent properties and organic reactivity, *J. Phys. Org. Chem.*, 2005, **18**(4), 275–297.
12 T. Welton, Room-temperature ionic liquids. Solvents for synthesis and catalysis, *Chem. Rev.*, 1999, **99**(8), 2071–2084.
13 M. J. Earle, *et al.*, The distillation and volatility of ionic liquids, *Nature*, 2006, **439**(7078), 831–834.
14 J. Lu, F. Yan and J. Texter, Advanced applications of ionic liquids in polymer science, *Prog. Polym. Sci.*, 2009, **34**(5), 431–448.
15 C. G. Yoo, Y. Pu and A. J. Ragauskas, Ionic liquids: Promising green solvents for lignocellulosic biomass utilization, *Curr. Opin. Green Sustainable Chem.*, 2017, **5**, 5–11.
16 H. Ohno, Electrolytes|ionic liquids, *Encyclopedia of Electrochemical Power Sources*, 2013, pp. 153–159.
17 W. Meindersma, *et al.*, Long term pilot plant experience on aromatics extraction with ionic liquids, *Sep. Sci. Technol.*, 2012, **47**(2), 337–345.
18 R. I. Canales and J. F. Brennecke, Comparison of ionic liquids to conventional organic solvents for extraction of aromatics from aliphatics, *J. Chem. Eng. Data*, 2016, **61**(5), 1685–1699.
19 M. Gras, *et al.*, Ionic-Liquid-Based Acidic Aqueous Biphasic Systems for Simultaneous Leaching and Extraction of Metallic Ions, *Angew. Chem., Int. Ed.*, 2018, **57**(6), 1563–1566.
20 X. Li, *et al.*, Ionic liquids with trichloride anions for oxidative dissolution of metals and alloys, *Chem. Commun.*, 2018, **54**(5), 475–478.
21 Y. Cai, *et al.*, Energy-efficient desalination by forward osmosis using responsive ionic liquid draw solutes, *Environ. Sci.:Water Res. Technol.*, 2015, **1**(3), 341–347.
22 C.-H. Hsu, *et al.*, Enhanced forward osmosis desalination with a hybrid ionic liquid/hydrogel thermoresponsive draw agent system, *ACS Omega*, 2019, **4**(2), 4296–4303.
23 A. Z. Haddad, *et al.*, Solar desalination using thermally responsive ionic liquids regenerated with a photonic heater, *Environ. Sci. Technol.*, 2021, **55**(5), 3260–3269.
24 Y. Kohno and H. Ohno, Temperature-responsive ionic liquid/water interfaces: relation between hydrophilicity of ions and dynamic phase change, *Phys. Chem. Chem. Phys.*, 2012, **14**(15), 5063–5070.
25 E. Kamio, *et al.*, Effect of temperature on the osmotic behavior of LCST type ionic liquid solutions as draw solutions in the forward osmosis process, *Sep. Purif. Technol.*, 2021, **275**, 119164.
26 E. Kamio, *et al.*, Fundamental investigation of osmolality, thermo-responsive phase diagram, and water-drawing ability of ionic-liquid-based draw solution for forward osmosis membrane process, *J. Membr. Sci.*, 2019, **570**, 93–102.
27 H. Iwasawa, *et al.*, Thermally Reversible On-Off Switching of Aggregation-Induced Emission *via* LCST Phase Transition of Ionic Liquids in Water (Advanced Optical Materials 20/2023), *Adv. Opt. Mater.*, 2023, **11**(20), 2370081.
28 Y. Kohno and H. Ohno, Ionic liquid/water mixtures: from hostility to conciliation, *Chem. Commun.*, 2012, **48**(57), 7119–7130.
29 Y. Kohno, Y. Deguchi and H. Ohno, Ionic liquid-derived charged polymers to show highly thermoresponsive LCST-type transition with water at desired temperatures, *Chem. Commun.*, 2012, **48**(97), 11883–11885.
30 S. Saita, *et al.*, Ammonium based zwitterions showing both LCST-and UCST-type phase transitions after mixing with water in a very narrow temperature range, *Chem. Commun.*, 2014, **50**(97), 15450–15452.
31 S. Saita, Y. Kohno and H. Ohno, Detection of small differences in the hydrophilicity of ions using the LCST-type phase transition of an ionic liquid–water mixture, *Chem. Commun.*, 2013, **49**(1), 93–95.
32 Y. Deguchi, N. Nakamura and H. Ohno, Thermoresponsive ionic liquid/water mixtures for separation and purification technologies, *Sep. Purif. Technol.*, 2020, **251**, 117286.
33 P. Paricaud, A. Galindo and G. Jackson, Understanding liquid-liquid immiscibility and LCST behaviour in polymer solutions with a Wertheim TPT1 description, *Mol. Phys.*, 2003, **101**(16), 2575–2600.
34 H. Kang, *et al.*, Molecular insight into the lower critical solution temperature transition of aqueous alkyl phosphonium benzene sulfonates, *Commun. Chem.*, 2019, **2**(1), 51.
35 M. J. Rosen and J. T. Kunjappu, *Surfactants and Interfacial Phenomena*, John Wiley & Sons, 2012.
36 Y. Cai, A critical review on draw solutes development for forward osmosis, *Desalination*, 2016, **391**, 16–29.
37 A. Rana and R. Y. Wang, Thermoresponsive liquid desiccants for dehumidification cycles, *Energy Convers. Manage.*, 2024, **301**, 118029.
38 X. Zhang, *et al.*, Low-grade heat-driven system utilizing thermo-responsive ionic liquid for greenhouses dehumidification and water recovery, *Appl. Therm. Eng.*, 2024, 123095.
39 J. D. Kocher, A. K. Menon and S. K. Yee. An air conditioning cycle using lower critical solution temperature mixtures, in *Heat Transfer Summer Conference*, American Society of Mechanical Engineers, 2023.
40 T. Takahashi, *et al.*, Control of phase transition temperature of thermoresponsive poly (ionic liquid) gels and application to a water purification system using these gels with polydopamine, *Sep. Purif. Technol.*, 2024, **337**, 126433.
41 S. Darvishmanesh, B. A. Pethica and S. Sundaresan, Forward osmosis using draw solutions manifesting liquid-liquid phase separation, *Desalination*, 2017, **421**, 23–31.
42 V. M. Egorov, *et al.*, Task-specific ionic liquid trioctylmethylammonium salicylate as extraction solvent for transition metal ions, *Talanta*, 2010, **80**(3), 1177–1182.
43 Q. Zhang, *et al.*, Thermoresponsive polymers with lower critical solution temperature: from fundamental aspects and measuring techniques to recommended turbidimetry conditions, *Mater. Horiz.*, 2017, **4**(2), 109–116.

44 I. Rodríguez-Escontrela, *et al.*, Characterization and phase behavior of the surfactant ionic liquid tributylmethylphosphonium dodecylsulfate for enhanced oil recovery, *Fluid Phase Equilib.*, 2016, **417**, 87–95.
45 F. Yan and J. Texter, Surfactant ionic liquid-based microemulsions for polymerization, *Chem. Commun.*, 2006, (25), 2696–2698.
46 R. Wang, *et al.*, Microemulsion-like aggregation behaviour of an LCST-type ionic liquid in water, *RSC Adv.*, 2014, **4**(27), 14055–14062.
47 Y. Zhao, *et al.*, Understanding the mechanism of LCST phase separation of mixed ionic liquids in water by MD simulations, *Phys. Chem. Chem. Phys.*, 2016, **18**(33), 23238–23245.
48 Y. Qiao, *et al.*, Temperature-responsive ionic liquids: fundamental behaviors and catalytic applications, *Chem. Rev.*, 2017, **117**(10), 6881–6928.
49 M. McEldrew, *et al.*, Ion clusters and networks in water-in-salt electrolytes, *J. Electrochem. Soc.*, 2021, **168**(5), 050514.
50 P. Yee, J. K. Shah and E. J. Maginn, State of hydrophobic and hydrophilic ionic liquids in aqueous solutions: are the ions fully dissociated?, *J. Phys. Chem. B*, 2013, **117**(41), 12556–12566.
51 N. C. Forero-Martinez, *et al.*, Water harvesting by thermoresponsive ionic liquids: A molecular dynamics study of the water absorption kinetics and of the role of nanostructuring, *J. Phys. Chem. B*, 2023, **127**(24), 5494–5508.
52 Y. Zhao, *et al.*, Effect of anionic structure on the LCST phase behavior of phosphonium ionic liquids in water, *Ind. Eng. Chem. Res.*, 2018, **57**(38), 12935–12941.

